www.setjournal.com

Effect of Soil Salinity on Thermal Behavior of Sandy Soils Under a Sahara Climate

Djihad Bennaceur¹, Nadia Laredj^{1,2}, Mustapha Maliki^{1,2}, Hanifi Misoum^{1,2}

¹Construction, Transportation and Environmental Protection Laboratory (LCTPE), Mostaganem 27000, Algeria.

² Faculty of science and technology, university Abdelhamid Ibn Badis, Mostaganem 27000, Algeria.

Abstract

Soil salinity represents a harmful environmental problem that occurs either naturally or as a consequence of ineffective management practices by humans, especially in arid regions. Assessing ground temperature profile represents an important indicator for evaluating the performance of geothermal systems, used in air conditioning of building. This paper proposes a conceptual and numerical model for predicting the hydrothermal behavior of unsaturated soils. The effect of soil salinity was investigated in this research. Two soil types (sandy and sandy loam) were studied under three salinity levels. Moreover, the arid meteorological conditions of Sahara Desert were considered in the developed model. According to the results, it appears that sandy soils exhibit optimal thermal behavior at a moderate salinity concentration of C = 0.1 M, with increased surface temperatures during warmer periods and better heat conservation in colder conditions. Conversely, sandy loam soils respond most effectively at a higher salinity concentration of C = 0.2 M, particularly excelling in heat retention during the summer months. These results emphasize the intricate interaction between soil composition and salinity in regulating temperature patterns, providing important knowledge for enhancing soil management practices that are customized to particular soil types and environmental factors, with potential implications for geothermal applications.

Keywords: salinity, thermal conductivity, unsaturated soil, heat transfer, salt concentration.

1. Introduction

In the last years, the ongoing population growth and the expansion of building infrastructure led to the increase in energy demand worldwide. The adoption of higher living standards and increased demand for thermal comfort significantly drive-up energy consumption [1], [2], [3]. Assessing soil temperature variations represents a key factor governing geothermal applications for the production of building heating and cooling. Many researches have been carried out in order to investigate the performance of geothermal heat exchangers, since they represent an environmentally friendly energy source [3], [4], [5], [6], [7].

Understanding the soil thermal characteristics is crucial for assessing the energy transfer in the ground. In geothermal systems, close understanding of soil thermal conductivity allows to improve the design of ground heat exchangers, resulting in better efficiency of geothermal systems and providing effective energy flow [8], [9]. The main thermal parameters include thermal conductivity, thermal diffusivity, and the volumetric heat capacity of soils [7]. Thermal conductivity describes the rate at which heat flows through a unit area of soil in a given time, under a specific temperature gradient. Different approaches have been used to measure the thermal conductivity of different soils, investigating the impact of various involved parameters [7], [10], [11], [12], these studies highlighted that the thermal conductivity is greatly

affected by various soil parameters such as water content, mineralogy, organic matter, temperature and soil density [13]. Recently, it has been reported that there is a relationship between the salt concentration and the thermal conductivity of soil. Accordingly, predictive models were established to consider the correlation between soil salinity and thermal conductivity [9], [13], [14].

Several studies have been carried out in order to assess the temperature profiles in the soil. Thereby, different mathematical models have been established to depict the periodic variations in soil temperature at specific depths and times. Researchers [15] found that changes in ground temperature are influenced by aboveground environment, others [16] developed a model to predict ground temperature profiles, improving the energy balance equation with an empirical correlation. A numerical model was developed to describe heat and mass transfer in soil at shallow depths and under a temperate climate [17]. The developed model incorporates the effects of soil moisture content to assess the soil thermal and physical characteristics. A study was carried out in which organic matter and thermal conductivity calculations were considered [18]. The numerical simulation results demonstrate a moderate tendency for ground temperature variations over extended durations. Some studies [5] demonstrate that is necessary to consider the atmospheresoil interaction to assess ground temperature variations at shallow depth for horizontal heat exchanger; since it contributes to improve the performance of geothermal systems.

At last, various models have been developed to predict the soil temperature profile. However, these models neglect the salt concentration in soil, making thus their application and validity limited. The climate change has contributed to the widespread growth of salt-affected soils around the world, especially in arid and semi-arid regions [19]. Recent research has shown that over one billion hectares of land are affected by soil salinization, with a potential increase of 10 to 16% per year [20].

The aim of this study is to investigate the effects of salinity on two different soil types in geothermal applications, and to better understand the impact of salt content on the heat transfer performance of salt-affected soils. In this work, a numerical model was developed to assess the annual fluctuations of the ground temperature

profile in the Sahara region, characterized by high solar radiation and significant daily temperature variations throughout the year 2023. The developed numerical framework also includes the atmospheric-soil interaction by considering the meteorological conditions of the studied arid region. A range of unsaturated soil types was analysed, with various salt concentrations, to investigate changes in soil temperature profiles and their implications for geothermal efficiency.

2. Model Development

2.1. Energy balance equations at the soil atmosphere boundary

The energy balance at the ground surface is calculated as follows [17]:

$$R_n + H - LE = G \tag{1}$$

Where R_n is the net radiation, H and LE are the sensible and latent heat flux, respectively, and G is the ground heat flux, all measured in W/m², and represented in Figure 1.

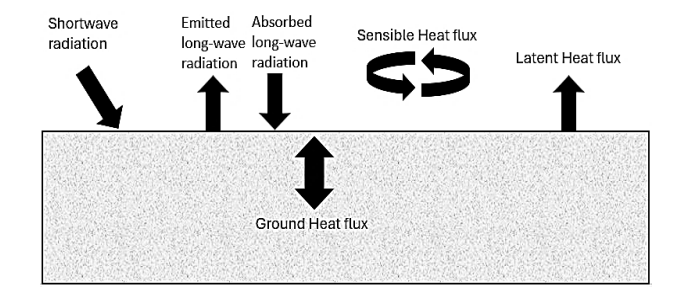


Figure 1. Energy transfer processes at the ground surface.

Direct and diffuse radiation are the two primary forms of solar radiation. While diffuse radiation travels through the atmosphere and is scattered by dust, water vapor, and clouds, direct radiation reaches the Earth's surface freely. Both kinds of radiation fall under the shortwave energy category. On the other hand, long-wave radiation is released by the Earth's surface and atmosphere. The balance of incoming and outgoing long-wave radiation, along with short-wave radiation that has been absorbed and reflected, is R_n . It can be calculated as follows [21]:

$$R_n = (1 - a_l)R_s - L \uparrow + L \downarrow \tag{2}$$

Where a_l represents the soil surface albedo, R_s refers to the short-wave radiation.

$$L \uparrow = \varepsilon_{\rm S} \, \sigma \, T_{\rm S}^4 \tag{3}$$

$$L \downarrow = \varepsilon_a \ \sigma \ T_a^4 \tag{4}$$

 $L\uparrow$ and $L\downarrow$, which represent the long-wave radiation emitted by the Earth's surface and the sky respectively, are calculated using the Stefan-Boltzmann law. The soil surface emissivity and air emissivity are represented by ε_s and ε_a , respectively. Additionally, the Stefan-Boltzmann constant is denoted by $\sigma=5.67\times 10^{-8}$ (Wm⁻² K⁻⁴), while T_s and T_a refer to the soil temperature and ambient temperature (K), respectively.

$$\varepsilon_a = 0.7 + 5.95 \times 10^{-4} e_a e^{1500/(T_a + 273.1)}$$
 (5)

$$e_a = \frac{RH}{100} e_s \tag{6}$$

$$e_{\rm s} = 0.6107 \, e^{17.269T_a/(T_a + 273.1)} \tag{7}$$

Where there is relative humidity, RH is expressed as a percentage, e_a represents the vapor pressure (kPa), and e_s indicates the saturated vapor pressure (kPa) at the ambient temperature T_a .

 R_s is calculated as follows:

$$R_s = (0.75 + 0.00002z) R_a \tag{8}$$

Where z represents the elevation above sea level (m) and R_a is the extraterrestrial solar radiation (W/m²) which are determined by [22]:

$$R_{\alpha} = G_{SC} d_{r} [\omega_{S} \sin \varphi \sin \delta + \cos \varphi \cos \delta_{S} \sin \omega_{S}]$$
 (9)

The solar constant G_{SC} is equal to 1367 W/m². φ and δ_s represent latitude and solar declination, respectively, while ω_S corresponds to the sunset hour angle, and the relative distance between the Earth and the Sun is denoted by dr.

$$d_r = 1 + 0.033 \cos\left(\frac{2\pi}{365}J\right) \tag{10}$$

$$\omega_{s} = \arccos[-\tan(\varphi)\tan(\delta_{s})] \tag{11}$$

$$\delta_s = 0.409 sin\left(\frac{2\pi}{365}J - 1.39\right) \tag{12}$$

The convective heat transfer between the ground surface and the surrounding air is represented by the sensible heat flux, which is computed as follows [23]:

$$H = \frac{\rho_a C_{p-a} (T_a - T_s)}{r_a} \tag{13}$$

Air density is denoted by ρ_a , heat capacity is represented by C_{p-a} , and aerodynamic resistance to heat transfer is expressed as r_a which is calculated as follow [24]:

$$r_a = \frac{\ln\left(\frac{Z_m - d}{Z_{om}}\right) \times \ln\left(\frac{Z_m - d}{Z_{oh}}\right)}{K^2 U_{Wind}} \tag{14}$$

 Z_m represents the height above the ground where wind speed, air temperature, and humidity are measured. U_{Wind} denotes the wind speed, while K is the von Karman constant. d is the fictive ground surface where the wind speed is zero.

$$d = \frac{2h_C}{3} \tag{15}$$

 h_c is the vegetation height, Z_{om} is the roughness length for momentum transfer, calculated by:

$$Z_{om} = 0.123h_{\mathcal{C}} \tag{16}$$

 Z_{oh} is the roughness length for vapor transfer:

$$Z_{oh} = 0.1 Z_{om} (17)$$

The latent heat flux LE is the interaction of the latent heat of vaporization L and the rate of evaporation E. The evaporation potential E_P at the soil surface is calculated assuming an unlimited water supply. The Penman-Monteith equation determines the value of E_P [22]

$$E = P \times \left[1 + \left(\frac{E_P}{P}\right)^{-2}\right]^{-\frac{1}{2}} \tag{18}$$

P represents the precipitation rate (mm/s).

$$E_{P} = \frac{1}{L} \left[\frac{\Delta \times R_{n} + \frac{\rho_{a} C_{pa}(e_{s} - e_{a})}{r_{a}}}{\Delta + \delta \left(1 + \frac{r_{c}}{r_{a}}\right)} \right]$$
(19)

The slope of the saturation vapor pressure curve is represented by Δ (kPa/K), the psychrometric constant is denoted by δ (kPa/K), and the canopy resistance is indicated by r_c (s/m).

2.2. Hydraulic flow in unsaturated soils

The Richards equation is used to determine the hydraulic transfer in an unsaturated soil as follows [25].

$$C(h)\frac{\partial h}{\partial t} - \nabla K(h)\nabla h - \frac{\partial K}{\partial z} = 0$$
 (20)

The specific moisture capacity, as a function of water content, is given by the equation $C(h) = \frac{\partial \theta}{\partial h}$, where h represents the suction head (m), and K(h) is the unsaturated hydraulic conductivity. The Mualem-van Genuchten formulation was selected for the functions K(h) and $\theta(h)$ [26], [27]

$$\theta(h) = \theta_r + (\theta_s - \theta_r)[1 + (\alpha h)^n]^{-m} \tag{21}$$

$$K(h) = K_s S_e^l \left[1 - (1 - S_e^{l/m})^m \right]^2$$
 (22)

$$S_e = \frac{\theta - \theta_r}{\theta_s - \theta_r} \tag{23}$$

The volumetric soil water content θ is measured in m³/m³, with θ_r and θ_s representing the residual and saturated water contents, respectively. The effective degree of saturation is denoted by S_e , while K_s refers to the saturated hydraulic conductivity (m/s). The empirical parameters α (kPa⁻¹), -1, n, and m are related by the equation m = 1 - 1/n [28].

2.3. Thermal transfer in unsaturated soils

The equation governing energy conservation in the soil is expressed as [5]

$$\rho_{s}c_{p-s}\frac{\partial T_{s}}{\partial t} = \nabla(k_{s}\nabla T_{s}) + \nabla(\rho_{w}c_{p-w}u_{w}T_{s}) + Q_{s}$$
(24)

Where ρ_s and ρ_w represent the densities of soil and water, respectively (kg/m³), c_{p-s} and c_{p-w} denote the heat capacities of soil and water, respectively (J/kg/K), and k_s stands for the soil's thermal conductivity. u_w represents the velocity of water within the soil (m/s), and Q_s refers to the heat source within the soil (W/m³).

The soil volumetric heat capacities were obtained using the following formulation [29]

$$C_v = \rho_d c_{n-s} + \rho_w c_{n-w} \theta \tag{25}$$

In this study, the thermal conductivities of the studied soils were determined based on varying water content and salinity levels. Two different soil types were investigated for three salinity concentrations. The aim is to evaluate the impact of salinity on soil temperature variations in arid regions. The thermal conductivity as function of water content and salt concentration is represented as follows [30]:

$$k_s = (A_1 \theta^2 + B_1 \theta)C^2 + (A_2 \theta^2 + B_2 \theta)C + (A_3 \theta^2 + B_3 \theta)$$
 (26)

Where C represents the salinity, and θ denotes the water content. A and B are empirical parameters that vary based on the soil type [30].

3. Characterization of the Study Region

3.1. Location and Geography

Adrar is located in southern Algeria, inside the immense expanse of the Sahara Desert, at around 27.87° N latitude and 0.29° W longitude, as seen in Figure 2. The region covers around 427,368 km² and is characterized by desert landscapes, including large sand dunes, rocky plateaus, and dry plains. The average height is roughly 258 meters above sea level. The sand, which is mostly made up of fine quartz grains, generates towering dunes that reach several hundred meters and are constantly changed by powerful desert winds. Adrar has a harsh desert environment, with summer temperatures regularly topping 45°C and little precipitation. This volatile and severe climate, together with its underlying geology, provide opportunities for geothermal energy exploration. High thermal gradients under the surface may allow for sustained heat extraction, making Adrar an attractive choice for renewable energy development in Algeria.

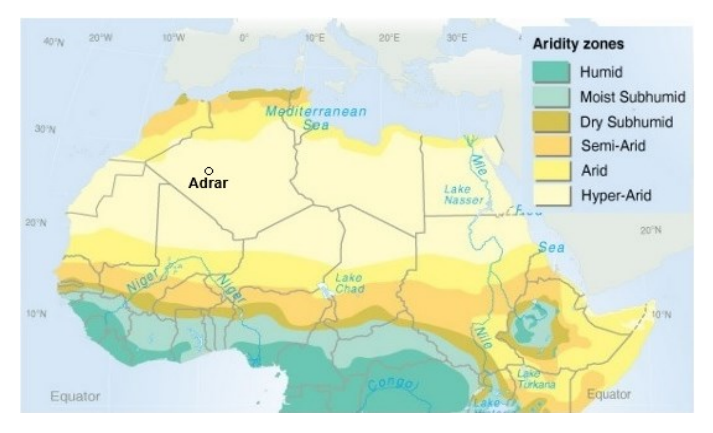


Figure 2. Geographic location of Adrar region within the aridity zones of northern Africa [source: World Meteorological Organization – WMO].

3.2. Overview of the climatic conditions

Adrar has a harsh desert environment, with very high temperatures, low humidity, and little rainfall. In summer, temperatures in Adrar can reach 48°C, with normal highs ranging from 40°C to 45°C. During the winter, temperatures are gentler, with average lows ranging from 10°C to 15°C, while overnight temperatures can occasionally drop below freezing, despite these seasonal changes, the region has an average yearly temperature of around 27°C. Figure 3 illustrates the maximum, average and minimum temperatures of the year.

Adrar's humidity is often low, frequently dipping below 20%, which, paired with high temperatures, adds to the dry conditions. Wind plays a crucial role in Adrar, with typical wind speeds ranging from 20 to 30 km/h. These winds, especially in the spring, may cause frequent and powerful sandstorms, which affect the region's landscape.

Adrar receives less than 5 mm of precipitation per year on average, making it one of Algeria's driest regions. Rainfall is typically in the form of brief, powerful storms that can cause flash floods in normally dry riverbeds (wadis). Extreme heat, low humidity, high winds, and little rainfall characterize Adrar's severe desert environment.

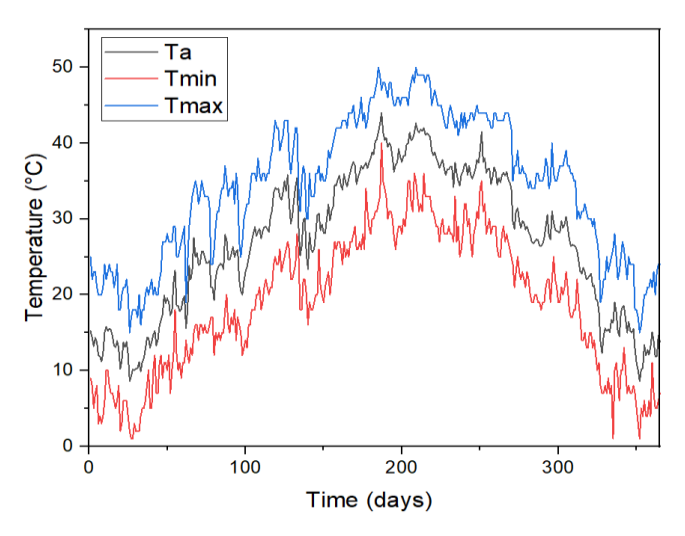


Figure 3. Yearly temperature variations in Adrar during the year 2023: Maximum, Average, and Minimum.

In this region, the combination of low precipitation and high evaporation rates led to increased salinity in soils. Moreover, soil salinization is proportional with piezometric level of water table depth [31]. The poor management practices caused by humans worsened the situation further in the last years.

4. Application of the Developed Numerical Model

The coupled partial differential equations outlined in Section 2 were numerically solved using the time-dependent solver in COMSOL Multiphysics. The study focused on two soil types, sand and sandy loam, and examined three salinity levels (no salinity, 0.1 M, and 0.2 M) applied at 40 cm below the surface to assess the impact of salinity on soil temperature profiles during the year

2023. The objective was to determine which soil type performs best under each salinity level, considering arid meteorological conditions and specific soil properties. The hydro-thermal properties of the investigated soils are presented in Table 1.

Climate variables are described as time-dependent parameters in the extended model. Table 2 summarizes the parameters used to compute the energy balance at the soil-atmosphere interface.

Table 1. Hydrothermal Properties of the Studied Soils.

Soil Type	Sand	Sandy loam
l	0.5	0.5
$\alpha (1/m)$	3.28	2.6
n_I	1.54	1.52
$ heta_r$	0.01	0.02
Ks (m/s)	2.5×10^{-5}	1.78×10^{-5}
$\rho_d (\text{kg/m}^3)$	1520	1600
$\mathbf{c}_{p\text{-}s}(\mathrm{Jkg}^{\text{-}1}\mathrm{K}^{\text{-}1})$	910	1040[32]

Table 2. Parameters for Calculating the Ground Surface Energy Balance.

Parameter	Value	
h_c	0.05 m	
Z_m	2 m	
U_{Wind}	5.25 m/s	
K	0.41	
P	9808844.7 Pa	
$c_{p ext{-}a}$	1004.7 Jkg ⁻¹ K ⁻¹	
$egin{aligned} \mathcal{C}_{p ext{-}w} \end{aligned}$	4181 Jkg ⁻¹ K ⁻¹	
L	$2.257 \times 10^{3} \text{J/kg}$	
a_l	0.18	

The computational domain under study spans a depth of 20 meters and a width of 10 meters. As shown in Figure 4, the soil domain is discretized into 3148 triangular elements, along with 150 edge elements and 4 vertex elements.

The boundary conditions for the soil model include specific hydraulic and thermal conditions at different locations. At the top surface, Neumann conditions are applied for both hydraulic and thermal aspects, representing a specified flux. The lateral boundaries are treated as adiabatic, meaning no heat or moisture transfer occurs. At the bottom, Dirichlet conditions are set, with a fixed pressure head for hydraulic conditions and a constant temperature for thermal conditions.

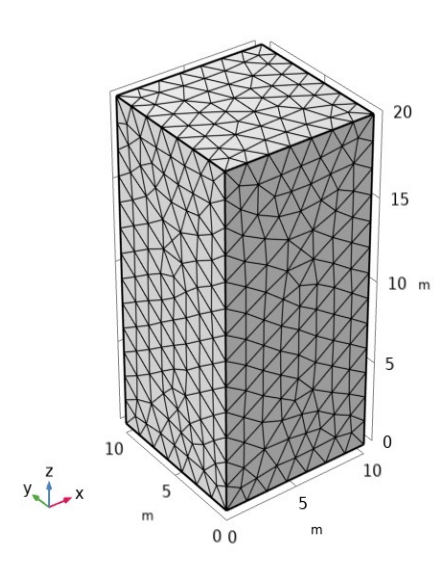


Figure 4. Meshing of the model domain.

5. Results and Discussion

After establishing the initial temperature profile and determining the fluxes for each soil type with varying salinity levels, the study shifts its focus to analyzing soil temperatures at different depths.

The seasonal surface variation in soil temperature for sandy soil with different salinity levels C = 0 M, C = 0.1 M, C = 0.2 M are illustrated in Figure 5. The highest peak temperature value was obtained on sand with C = 0.1 M in the summer follower by C = 0 M and C = 0.2 M. On the other hand, the trend is reversed in winter, the sand at C = 0 M holds heat better, this leads to the conclusion that salinity affects the thermal behavior of sand differently throughout the year, with moderate salinity enhancing heat retention in summer, while non-saline soils retain more heat in winter.

Figure 6 depicts the seasonal change in surface temperature for sandy loam soils with varying salinity levels C = 0 M, C = 0.1 M, and C = 0.2 M throughout the year. All soils have a sinusoidal temperature pattern, with the maximum temperatures occurring mid-year and the lowest at both the beginning and end of the year. The soil with the highest salinity C = 0.2 M has the highest peak temperature during the summer, slightly surpassing both moderate salinity C = 0.1 M and non-saline C = 0 M soils. This shows that increasing salinity improves soil heat retention during warmer months. Despite these variances, overall temperature trends are similar, indicating that salinity has the greatest influence on peak summer temperatures in sandy loam soils.

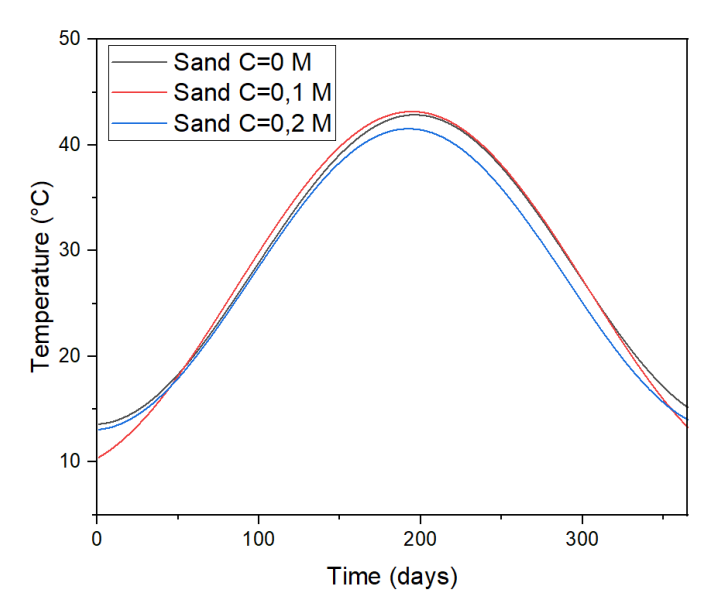


Figure 5. Seasonal surface temperature variation for sandy soil with different salinity levels (C = 0 M, C = 0.1 M, C = 0.2 M)

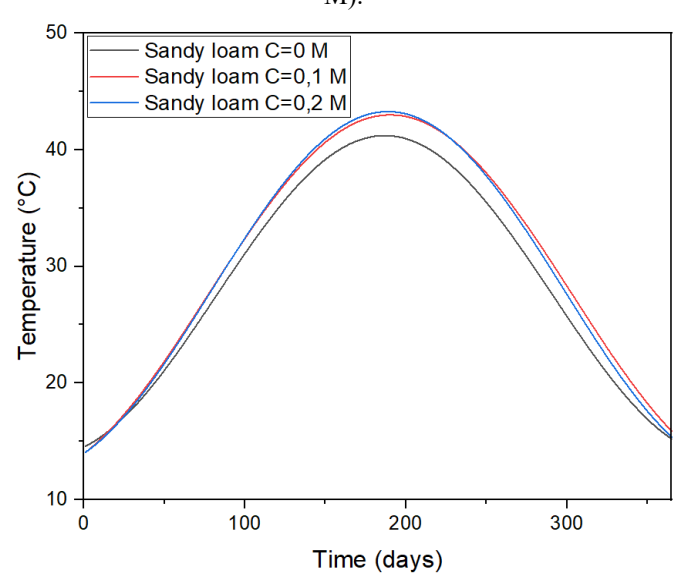


Figure 6. seasonal surface temperature variation for sandy loam soil with different salinity levels (C = 0 M, C = 0.1 M, C = 0.2 M).

Figure 7 shows the variation in seasonal temperatures at 20 cm depth of sandy soils of the three levels of salinity. During summer, the peak temperature is attained by the soil with moderate salinity corresponding to C = 0.1 M, followed by the non-saline soil corresponding to C = 0.2 M takes the third position. In contrast, during winter, non-saline soil, C = 0 M, shows the maximum temperature, followed by highly saline soil, C = 0.2 M, while the minimum of the three will correspond to the soil with moderate salinity, C = 0.1 M. These variations reveal that salinity levels influence soil temperature differently in warm and

cold seasons, with moderate salinity leading to higher summer temperatures, while non-saline soil retains more heat during the winter months.

At the same depth, Figure 8 illustrates the seasonal temperature variation in sandy loam soils, comparing three salinity levels. In both summer and winter, the soil with the highest salinity C=0.2~M had the highest temperature, demonstrating that increasing salinity improves the soil's capacity to absorb heat. This is followed by moderately salty soil C=0.1~M, and nonsaline soil C=0~M, which has the lowest peak temperature. This trend indicates that salinity plays an important role in altering the soil's temperature.

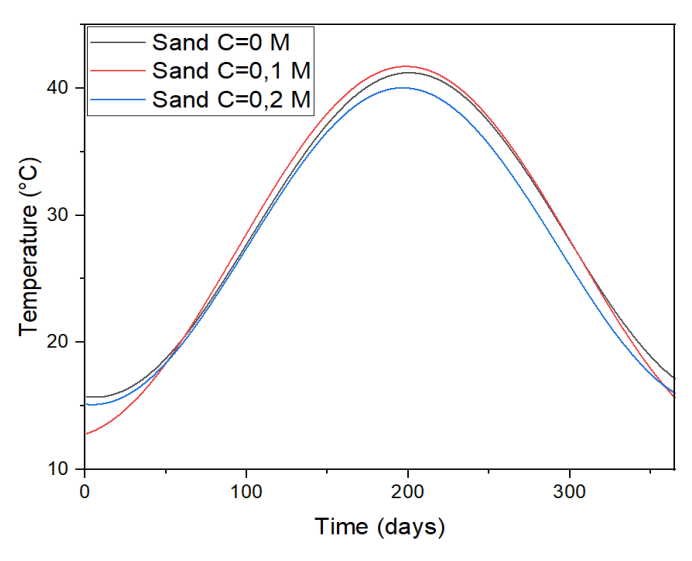


Figure 7. Seasonal temperature fluctuations at 20 cm depth in sand soil with varying salinity Levels (C = 0 M, C = 0.1 M, C = 0.2 M).

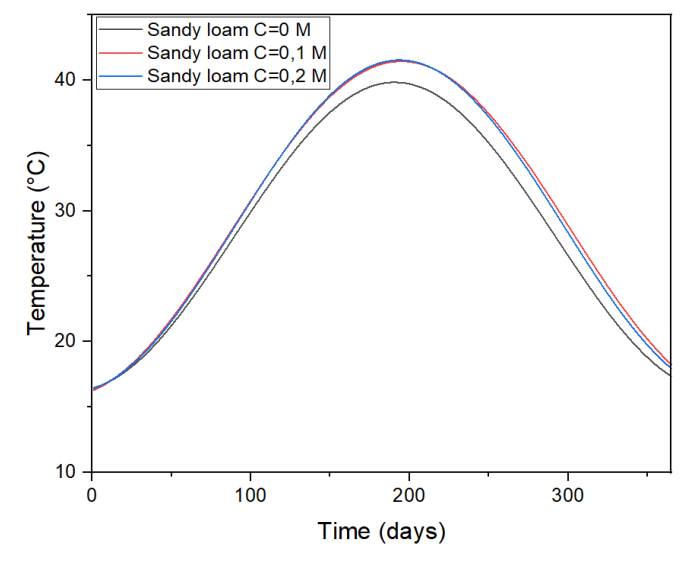


Figure 8. Seasonal temperature fluctuations at 20 cm depth in sandy loam soil with varying salinity levels (C = 0 M, C = 0.1 M, C = 0.2 M).

At a depth of 40 cm, where salinity is present, the seasonal fluctuation of temperature in sandy soil over a year for three different levels of salinity is illustrated in Figure 9, following the same pattern as Figures 5 and Figure 7. The temperature peaks in the summer, with the highest value in soil with C = 0.1 M, followed by soil with C = 0 M, and finally soil with C = 0.2 M. However, during the winter period, the highest temperature is recorded in soil with C = 0 M, followed by soil with C = 0.2 M, and lastly, soil with C = 0.1 M.

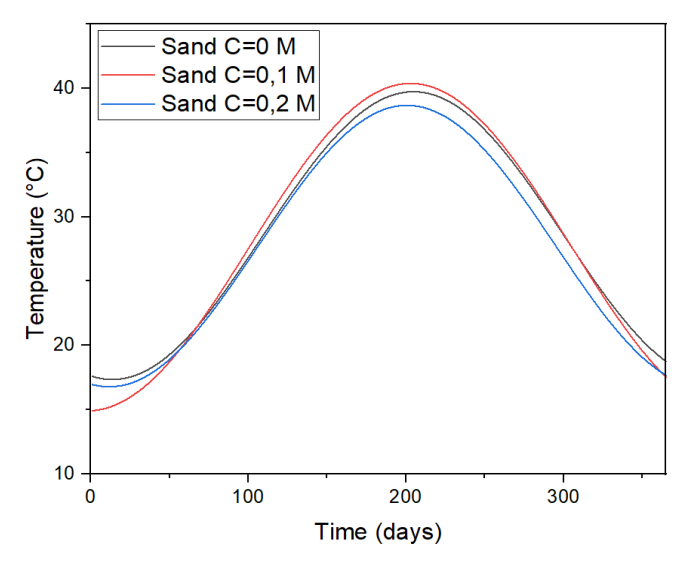


Figure 9. Seasonal temperature fluctuations at 40 cm depth in sandy soil with varying salinity levels (C = 0 M, C = 0.1 M, C = 0.2 M).

At an equivalent depth, the seasonal temperature fluctuations in sandy loam soil over a year for three different salinity levels are displayed in Figure 10. The results are consistent with those shown in Figures 6 and Figure 8, indicating that as salinity increases, so does the temperature. Specifically, soil with the highest salinity C = 0.2 M exhibits the highest temperatures throughout the year, followed by soil with C = 0.1 M and C = 0 M. The trend is most noticeable during the summer months when the temperature peaks are more pronounced, with higher salinity levels leading to greater heat retention.

Figure 11 illustrates the temperature profile in sandy soil at various depths for different salinity levels, during winter (January) and summer (June) of the year 2023, with salinity implemented only at the surface down to a depth of 40 cm in the model. The temperature variation is most pronounced near the surface, particularly in June, where salinity is $C = 0.1 \, M$ leads to slightly higher temperatures compared to salinity levels $C = 0 \, M$ and $C = 0 \,$

0.2 M. In January, temperature differences due to salinity are minimal, indicating that salinity has a stronger effect during warmer periods. Below the depth of 40 cm, where salinity is not applied, the temperature stabilizes at around 25°C. Overall, salinity influences surface temperatures more in summer, with less impact during winter.

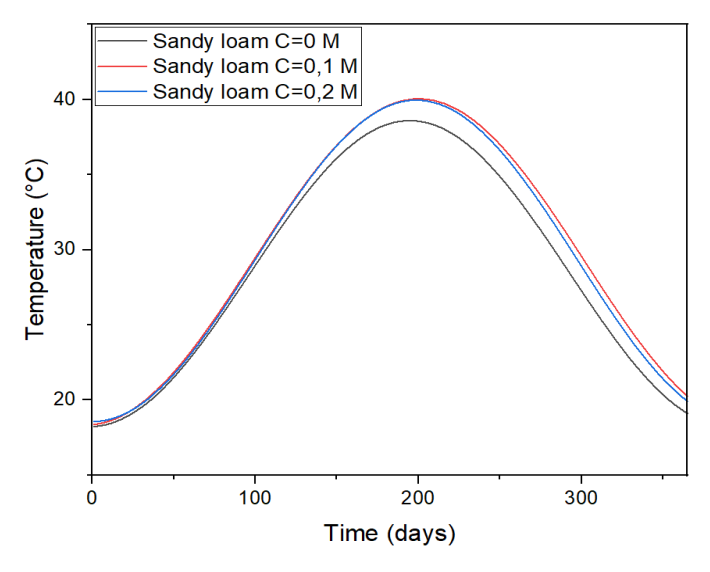


Figure 10. Seasonal temperature fluctuations at 40 cm depth in sandy loam soil with varying salinity levels (C = 0 M, C = 0.1 M, C = 0.2 M).

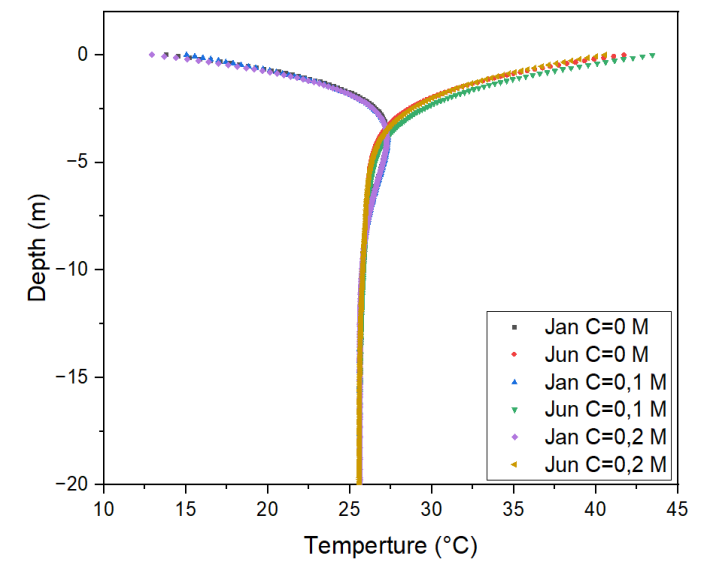


Figure 11. Temperature profile with depth for sandy soil for varying salinity levels (C = 0 M, C = 0.1 M, C = 0.2 M).

Figure 12 illustrates the temperature profile in sandy loam soil at various depths for different salinity during winter (January) and summer (June), with salinity applied only to the top 40 cm of the soil. In this upper layer, temperature differences are most pronounced, especially during the summer (June), where soil with higher salinity $C = 0.2 \, \text{M}$ exhibits higher temperatures. In winter

(January), the temperature differences between salinity levels are less noticeable, with slightly higher temperatures in non-saline soil C = 0 M. Below the 40 cm depth, where salinity is not applied, the temperature stabilizes across all salinity levels and remains consistent around 25°C, showing no significant seasonal or salinity influence. This indicates that salinity affects the temperature primarily near the surface, with a greater impact during warmer periods, while deeper soil layers maintain a stable temperature profile independent of salinity.

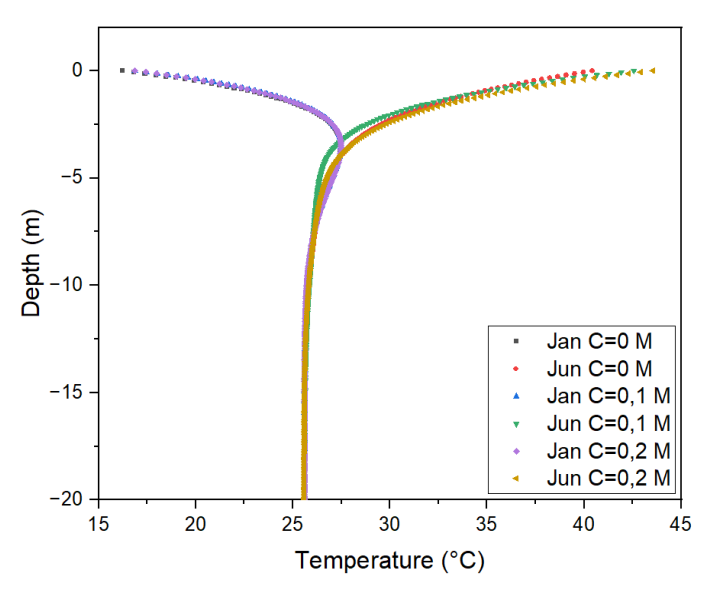


Figure 12. Temperature Profile with depth for sandy loam soil for varying salinity levels (C = 0 M, C = 0.1 M, C = 0.2 M).

6. Conclusion

This research paper presents a numerical model of soil temperature variations in Sahara Desert conditions. Two different soil types: sand and sandy loam, were investigated, under three levels of salinity C = 0 M, C = 0.1 M, and C = 0.2 M in Adrar region of Algeria during the year 2023. The finding reveals that in sandy soils, a salinity level of C = 0.1 M offers the best thermal performance, leading to higher surface temperatures during warmer months while maintaining moderate heat retention in colder conditions. For sandy loam soils, the highest salinity level C = 0.2 M proved to be the most effective in retaining heat, particularly during the summer, resulting in higher surface temperatures. This study highlights the varying impact of salinity on different soil types, with sandy soils responding best to moderate salinity, while sandy loam benefits more from higher salinity levels. These findings are crucial for geothermal applications as they highlight the interaction between soil salinity, and temperature behavior. understanding could serve as a valuable guide for selecting the appropriate soil types and chemical treatments to enhance thermal conductivity and heat retention, which is essential for the development of efficient geothermal systems in arid regions such as the Sahara Desert. Moreover, future studies should aim to explore a more extensive range of soil types and salinity conditions, as this would significantly enhance our understanding of how geothermal systems perform in various environmental contexts. By investigating these factors across different arid regions, researchers can improve the applicability of geothermal energy solutions in diverse settings. This expanded knowledge base will ultimately contribute to the optimization of geothermal system designs, making them more efficient and better suited to the unique challenges posed by arid environments, thereby advancing the development of sustainable energy solutions that can meet the demands of such regions.

Competing Interest Statement

The authors declare no known competing financial interests or personal relationships that could have influenced the work reported in this paper.

Data Availability Statement

Supplementary materials and data used in this research are accessible upon request. For access, please contact the corresponding author via [mustafa.maliki@univ-mosta.dz].

Author Contribution Roles

- Djihad Bennaceur: Conceptualization, Software, Investigation, Writing Original Draft.
- Nadia Laredj: Methodology, Investigation, Resources.
- Mustapha Maliki: Methodology, Software, Project administration.
- Hanifi Missoum: Conceptualization, Supervision.

Nomenclature

- R_n Net radiation, W/m²
- H Sensible heat flux, W/m²
- G Ground heat transfer, W/m^2
- R_s Shortwave radiation, W/m²
- E Evapotranspiration rate
- L Latent heat of vaporization of water, J/kg
- LE Latent heat flux, W/m²
- a_l The surface albedo
- R_a Longwave radiation, W/m²
- σ Stefan-Boltzman constant, Wm⁻²K⁻⁴
- ε Emissivity of the surface
- T_a Ambient temperature, K
- T_s Soil temperature, K
- r_a The aerodynamic heat resistance, s/m
- C(h) The specific moisture capacity
- H The suction head, m
- *K(h)* The unsaturated hydraulic conductivity, m/s
- K_s The saturation hydraulic conductivity, m/s
- S_e The effective degree of saturation
- θ The volumetric soil water content, m³/m³
- θ_r The residual water contents, m³/m³
- θ_s The saturated water contents, m³/m³
- α Van Genuchten empirical shape parameter, m⁻¹
 - ρ_s The soil density, kg/m³
- ρ_w The water density, kg/m³
- ρ_d The soil dry density, kg/m³
- ρ_a The density of the air, kg/m³
- c_p . The specific heat capacity of water, Jkg⁻¹K⁻¹
- c_{p-} The specific heat capacity of soil, Jkg⁻¹K⁻¹
- c_{p-} The specific heat capacity of the air, Jkg⁻¹K⁻¹
- u_w The soil water velocity, m/s
- k_s The soil thermal conductivity, Wm⁻¹K⁻¹
- C_v The soil volumetric heat capacity, Jm^3K^1

References

- [1] E. Uzlu, "Application des réseaux neuronaux artificiels formés par l'algorithme Jaya pour la prévision de la consommation d'énergie en Turquie," *Sources d'énergie, Partie B : Économie, Planification et Politique*, vol. 14, no. 5, pp. 183–200, 2019.
- [2] C. Mokhtara, B. Negrou, N. Settou, A. Bouferrouk, and Y. Yao, "Optimal design of grid-connected rooftop PV systems: An overview and a new approach with application to educational buildings in arid climates," *Sustainable Energy Technologies and Assessments*, vol. 47, Oct. 2021, doi: 10.1016/j.seta.2021.101468.
- [3] M. Benhammou, L. Boubekeur, H. Moungar, and Y. Sahli, "Performance assessment of a novel type of Earth-to-Air Heat Exchanger consisting of a composite pipe integrating a convective zone for summer cooling of buildings," *J Energy Storage*, vol. 62, Jun. 2023, doi: 10.1016/j.est.2023.106890.
- [4] W. Gao, S. Masum, J. Black, and H. R. Thomas, "Improving computational efficiency of numerical modelling of horizontal ground source heat pump systems for accommodating complex and realistic atmospheric processes," *Geothermics*, vol. 106, Dec. 2022, doi: 10.1016/j.geothermics.2022.102568.
- [5] F. Tang and H. Nowamooz, "Outlet temperatures of a slinky-type Horizontal Ground Heat Exchanger with the atmosphere-soil interaction," *Renew Energy*, vol. 146, pp. 705–718, Feb. 2020, doi: 10.1016/j.renene.2019.07.029.
- [6] M. Ouzzane, M. T. Naqash, and O. Harireche, "Assessment of the Potential Use of Shallow Geothermal Energy Source for Air Heating and Cooling in the Kingdom of Saudi Arabia," *Nature Environment* and Pollution Technology, vol. 20, no. 5, pp. 1923– 1934, Dec. 2021, doi: 10.46488/NEPT.2021.V20I05.008.
- [7] Y. Xu, Y. Chen, J. Li, and W. Zang, "Study on the effect of ground stratification on heat transfer of vertical ground heat exchangers in lateritic clay areas," *Appl Therm Eng*, vol. 253, Sep. 2024, doi: 10.1016/j.applthermaleng.2024.123804.
- [8] G. S. Jia, Z. Y. Tao, X. Z. Meng, C. F. Ma, J. C. Chai, and L. W. Jin, "Review of effective thermal conductivity models of rock-soil for geothermal energy applications," Jan. 01, 2019, *Elsevier Ltd.* doi: 10.1016/j.geothermics.2018.08.001.
- [9] O. Kolawole, S. Rehmatullah, and V. Shah, "Evaluating soil thermal conductivity for buried infrastructure: Impact of water salinity, mineral composition, and moisture content on heat transfer," *Progress in Engineering Science*, vol. 1, no. 2–3, p. 100014, Oct. 2024, doi: 10.1016/j.pes.2024.100014.
- [10] F. Q. Cui, Z. Y. Liu, J. B. Chen, Y. H. Dong, L. Jin, and H. Peng, "Experimental test and prediction model of soil thermal conductivity in permafrost regions,"

- Applied Sciences (Switzerland), vol. 10, no. 7, Apr. 2020, doi: 10.3390/app10072476.
- [11] H. He, L. Liu, M. Dyck, B. Si, and J. Lv, "Modelling dry soil thermal conductivity," *Soil Tillage Res*, vol. 213, Sep. 2021, doi: 10.1016/j.still.2021.105093.
- [12] N. Kardani, A. Bardhan, P. Samui, M. Nazem, P. G. Asteris, and A. Zhou, "Predicting the thermal conductivity of soils using integrated approach of ANN and PSO with adaptive and time-varying acceleration coefficients," *International Journal of Thermal Sciences*, vol. 173, Mar. 2022, doi: 10.1016/j.ijthermalsci.2021.107427.
- [13] Z. Ju, K. Guo, and X. Liu, "Modelling thermal conductivity on salt-affected soils and its modification," *International Journal of Thermal Sciences*, vol. 185, Mar. 2023, doi: 10.1016/j.ijthermalsci.2022.108071.
- [14] Z. Duan, X. Yan, Q. Sun, X. Tan, and C. Dong, "Effects of water content and salt content on electrical resistivity of loess," *Environ Earth Sci*, vol. 80, no. 14, Jul. 2021, doi: 10.1007/s12665-021-09769-2.
- [15] R. Garcia Gonzalez, A. Verhoef, P. L. Vidale, B. Main, G. Gan, and Y. Wu, "Interactions between the physical soil environment and a horizontal ground coupled heat pump, for a domestic site in the UK," *Renew Energy*, vol. 44, pp. 141–153, Aug. 2012, doi: 10.1016/j.renene.2012.01.080.
- [16] M. Badache, P. Eslami-Nejad, M. Ouzzane, Z. Aidoun, and L. Lamarche, "A new modeling approach for improved ground temperature profile determination," *Renew Energy*, vol. 85, pp. 436–444, 2016, doi: 10.1016/j.renene.2015.06.020.
- [17] M. Chalhoub, M. Bernier, Y. Coquet, and M. Philippe, "A simple heat and moisture transfer model to predict ground temperature for shallow ground heat exchangers," *Renew Energy*, vol. 103, pp. 295–307, Apr. 2017, doi: 10.1016/j.renene.2016.11.027.
- [18] X. Fang, S. Luo, S. Lyu, C. Cheng, Z. Li, and S. Zhang, "Numerical modeling of the responses of soil temperature and soil moisture to climate change over the Tibetan Plateau, 1961–2010," *International Journal of Climatology*, vol. 41, no. 8, pp. 4134–4150, Jun. 2021, doi: 10.1002/joc.7062.
- [19] M. Maliki, F. Z. Hadjadj, N. Laredj, and H. Missoum, "Assessment and Correlation of Saline Soil Characteristics using Electrical Resistivity," *Journal of Electrochemical Science and Technology*, vol. 14, no. 3, pp. 205–214, Aug. 2023, doi: 10.33961/jecst.2022.00871.
- [20] F. Z. Hadjadj, N. Laredj, M. Maliki, and H. Missoum, "Influence of Electrokinetic Process on Compressibility Behaviour of Salt Affected Soils," *Geotechnical and Geological Engineering*, vol. 40, no. 8, pp. 4159–4170, Aug. 2022, doi: 10.1007/s10706-022-02147-0.
- [21] N. An, S. Hemmati, and Y. J. Cui, "Assessment of the methods for determining net radiation at different timescales of meteorological variables," *Journal of Rock Mechanics and Geotechnical Engineering*, vol. 9, no. 2,

- pp. 239–246, Apr. 2017, doi: 10.1016/j.jrmge.2016.10.004.
- [22] L. S. Pereira, "Crop Evapotranspiration-Guidelines for computing crop water requirements-FAO Irrigation and drainage paper 56," 1998. [Online]. Available: https://www.researchgate.net/publication/235704197
- [23] W. Choi, R. Ooka, and Y. Nam, "Impact of long-term operation of ground-source heat pump on subsurface thermal state in urban areas," *Sustain Cities Soc*, vol. 38, pp. 429–439, Apr. 2018, doi: 10.1016/j.scs.2017.12.036.
- [24] R.G. Allen, A Penman for all seasons, vol. 4. 1986.
- [25] M. A. Celia, E. T. Bouloutas, and R. L. Zarba, "A General Mass-Conservative Numerical Solution for the Unsaturated Flow Equation," *Water Resour Res*, vol. 26, no. 7, pp. 1483–1496, 1990.
- [26] Y. Mualem, "Hydraulic Conductivity of Unsaturated Porous Media' Generalized Macroscopic Approach," *Watee Resources Research*, vol. 14, no. 2, pp. 325–334, 1978.
- [27] M. T. Van Genuchten, "A Closed-form Equation for Predicting the Hydraulic Conductivity of Unsaturated Soils 1," *SOIL SCI. SOC. AM. J.*, vol. 44, pp. 892–898, 1980.
- [28] Z. Tian, D. Kool, T. Ren, R. Horton, and J. L. Heitman, "Approaches for estimating unsaturated soil hydraulic

- conductivities at various bulk densities with the extended Mualem-van Genuchten model," *J Hydrol (Amst)*, vol. 572, pp. 719–731, May 2019, doi: 10.1016/j.jhydrol.2019.03.027.
- [29] K. A. Alnefaie and A.-H. H. Nidal, "Specific Heat and Volumetric Heat Capacity of Some Saudian Soils as affected by Moisture and Density," *International Journal of Materials*, vol. 7, pp. 42–46, Nov. 2020, doi: 10.46300/91018.2020.7.8.
- [30] K. Malek, K. Malek, and F. Khanmohammadi, "Response of soil thermal conductivity to various soil properties," *International Communications in Heat and Mass Transfer*, vol. 127, Oct. 2021, doi: 10.1016/j.icheatmasstransfer.2021.105516.
- [31] I. Recioui, M. D. Bouhoun, D. Boutoutaou, and A. Mihoub, "Spatial variation of the water rising and water table salinity in the Basin of Ouargla (Algerian Sahara)," in *Energy Procedia*, Elsevier Ltd, 2017, pp. 571–578. doi: 10.1016/j.egypro.2017.07.082.
- [32] J. Busby, "Determination of Thermal Properties for Horizontal Ground Collector Loops," in *Proceedings World Geothermal Congress*, Apr. 2015. [Online]. Available: http://badc.nerc.ac.uk/home